

# 9

## Analysis of EC2 Observations

### 9.1 Beam deconvolution

A summary of observations and detected line intensities,  $T_R^*$ , can be found in Figs. 8.5, 8.6, 8.7 and Table 9.2. However, before analysis can take place, the possible effects of beam dilution on measured line intensities (and rms values) must be taken into account. The effective aperture or half-power beam width,  $hpbw$ , often shortened to just ‘beam’, of a radio telescope is dictated by the Rayleigh Limit (Hecht 2002):

$$hpbw = 1.22\lambda/d, \quad (9.1)$$

where  $hpbw$  is measured in radians,  $\lambda$  is the observed wavelength, and  $d$  is the diameter of the antenna dish (with both lengths in the same units). Converting for a beam,  $\theta_b$ , in arc seconds, observed frequency,  $\nu$ , in GHz and an antenna diameter,  $d$ , in metres, yields the more useful formula:

$$\theta_b = 75443/\nu d. \quad (9.2)$$

By definition, if a telescope’s beam,  $\theta_b$ , is the same angular size as the Gaussian full width half power,  $fwhp$ , size of a given source,  $\theta_s$ , any detected peak intensity will be diluted by exactly 50 per cent. It follows that an indefinitely extended source ‘fills’ the beam completely and a source smaller than the beam underestimates the intensity by

## 9: ANALYSIS OF EC2 OBSERVATIONS

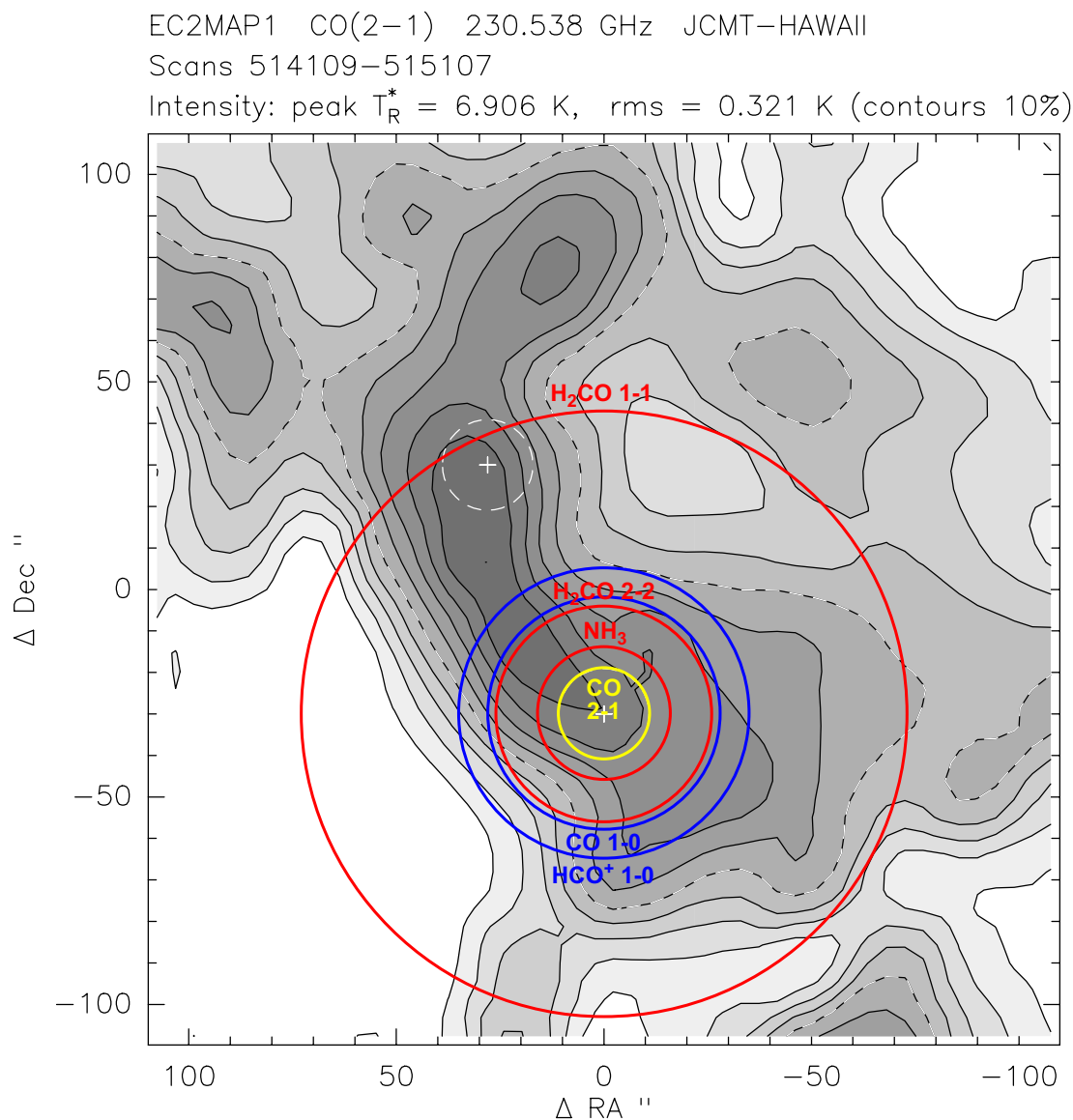


Figure 9.1: Telescope beam sizes centred on EC2 position A (Digel et al. 1994, copk1,  $\alpha_{1950} = 02:44:52.6$ ,  $\delta = 58:16:00.2$ , which is 30 arcsec below map centre) superimposed on JCMT EC2 map 1 of observed CO 2-1 spectra (axis offsets in arcsec). Colour key: Yellow = JCMT 15m; Blue = ARO 12m; Red = Effelsberg 100m. Contour levels 10% of peak, dashed contour is 50% of peak ( $fwhp$ ) and upper white circle denotes position J (Digel et al. 1994, copk2). See Appendix B for telescope beam sizes centred on EC2 position K.

more than 50 per cent. Therefore, I correct observed intensities,  $T_{\text{R}}^*$ , for beam dilution effects using:

$$T_{\text{mb}} = T_{\text{R}}^*/\eta_{\text{bf}}, \quad \text{with} \quad \eta_{\text{bf}} = \theta_{\text{s}}^2/(\theta_{\text{s}}^2 + \theta_{\text{b}}^2), \quad (9.3)$$

where  $\eta_{\text{bf}}$  is the beam filling correction factor (Wang et al. 2004). Table 9.2 also lists beam deconvolved line temperatures,  $T_{\text{mb}}$ , and  $\text{rms}_{\text{mb}}$  values, derived with equation 9.3 and appropriate values for  $\theta_{\text{b}}$  (equation 9.2) for each combination of telescope diameter and observed line frequency. Determination of an appropriate source size,  $\theta_{\text{s}}$ , is more difficult, as my CO maps (section 8.6) show EC2 to be clumpy and irregular in shape. Fig. 9.1 shows telescope beam sizes for transitions of  $\text{NH}_3$ ,  $\text{H}_2\text{CO}$ ,  $\text{HCO}^+$  and CO superimposed on JCMT EC2 map 1 of observed CO 2–1 spectra. As discussed in section 9.4 (below) observed line intensities were deconvolved with a cloud of size of  $150 \times 40 \text{ arcsec}^2$  for  $^{12}\text{CO}$ , and  $100 \times 30 \text{ arcsec}^2$  for  $^{13}\text{CO}$ ,  $\text{C}^{18}\text{O}$  and all other molecules.

It should be noted that for SO at 30 GHz the Effelsberg 100m beam is around 30 arcsec, as opposed to a calculated value of 25 arcsec. This is because the quality of the outer parts of the antenna, built in the early 1970s and initially only designed to reach 15 GHz, is not as good as that of the inner parts, which can observe up to 86 GHz. Thus the 30 GHz horn only collects radiation from the inner part of the primary dish, reducing the beam from 25 to 30 arcsec, but increasing the main beam efficiency.

## 9.2 Ammonia as a thermometer

Before estimating abundances of the observed molecular species, the main physical parameters of the gas have to be determined, i.e., its density and temperature. There are several tracers sensitive to both density and temperature, though none that only traces density and one that exclusively traces kinetic temperature.

According to Goldsmith and Langer (1999), the excitation temperature,  $T_{\text{ex}}$ , is defined by the relative populations or column densities of any two levels  $i$  and  $j$  of statistical weights  $g_i$  and  $g_j$  and energies  $E_i$  and  $E_j$  relative to an arbitrary common reference,

through

$$N_i = N_j \left( \frac{g_i}{g_j} \right) \frac{\exp(-E_i/kT_{\text{ex}})}{\exp(-E_j/kT_{\text{ex}})}, \quad (9.4)$$

where for a total column density,  $N$ , of the particular species of molecule, each state has a column density  $N_i$  such that  $N = \sum N_i$ . Since  $j$  is a constant in this sum (it refers to one fiducial level), it can be taken out of the sum, so that

$$N = \frac{N_j}{g_j \exp(-E_j/kT_{\text{ex}})} \sum g_i \exp(-E_i/kT_{\text{ex}}). \quad (9.5)$$

Since  $\sum g_i \exp(-E_i/kT_{\text{ex}})$  represents the sum over all  $i$ , it does not depend on  $i$  and can therefore be defined as  $Q$ , the partition function, i.e.

$$N = \frac{N_j Q}{g_j \exp(-E_j/kT_{\text{ex}})} \quad (9.6)$$

where the partition function,

$$Q = \sum g_i \exp(-E_i/kT_{\text{ex}}), \quad (9.7)$$

is true for a thermodynamically large system in local thermodynamic equilibrium (LTE), with temperature  $T_{\text{ex}}$ , a fixed volume and number of particles, and number of states  $i$ , each of energy  $E_i$ . It follows that if any two levels are connected by a radiative transition,  $T_{\text{ex}}$  can be directly measured, and in the case of a molecule in LTE, all excitation temperatures are the same, so the population of each level is given by

$$N_j = \frac{N}{Q} g_j \exp(-E_j/kT_{\text{ex}}). \quad (9.8)$$

For linear molecules in LTE with  $kT > hB_0$ , Goldsmith and Langer (1999) show that

$$Q = kT/hB_0, \quad (9.9)$$

where  $B_0$  is the rotational constant (since  $Q$  is dimensionless,  $k/h$  can be omitted if  $B_0$  is measured in the same units (K) as  $T$ ).

For cases of LTE the total molecular column density can be obtained from the column density of any individual transition if  $T$  is known. Conversely, if two (or more) column densities are known for individual transitions of the species, both the

temperature and the total column density can be determined from the column density ratios. Total column densities can also be derived from a suitable rotation diagram, where the slope of the line for normalised known column densities is  $-\log e/T_{\text{rot}}$ , using a weighted fit to total emission (where the weights reflect the signal to noise ratio).

Ammonia<sup>1</sup> is a suitable molecular cloud thermometer because relative populations of the different metastable ( $J=K$ ) inversion levels of  $\text{NH}_3$  are expected to be mainly determined by collisional processes, where they decay radiatively via slow  $\Delta K = \pm 3$  transitions, and thus reflect the kinetic temperature of the gas where  $T_{\text{rot}} \leq T_{\text{kin}}$  (Walmley and Ungerechts 1983). For para- $\text{NH}_3$ , dipole transitions between levels which have high Einstein A coefficient values ( $\sim 0.1 \text{ s}^{-1}$ ), have the selection rule  $\Delta K = 0$ , and hence the majority of interstellar  $\text{NH}_3$  molecules tend to exist in the metastable ( $J=K$ ) levels. Inversion splitting allows column densities in the various rotational levels to be determined and, due to the proximity of the inversion transitions in frequency, relative calibration errors should be small.

However, the tendency of the (1, 1) – (2, 2) rotational temperature to underestimate the kinetic temperature is a general property of  $\text{NH}_3$  metastable levels. Theoretical and experimental work aimed at determining collisional cross sections for rotational excitation of ammonia, by helium and molecular hydrogen, have been applied to the problem of determining the dependence of  $\text{NH}_3$  rotational temperatures upon kinetic temperature. With reliable collision rates between the lower rotational states of ammo-

---

<sup>1</sup>Ammonia ( $\text{NH}_3$ ) is a symmetric pyramidal molecule where the nitrogen atom spends most of its time some distance from the plane of the three hydrogen atoms. In the ground vibrational state, the nitrogen atom does not have sufficient energy to penetrate the plane of the hydrogen atoms. From a classical viewpoint, inversion cannot occur because the nitrogen atom does not have enough energy to get over the hindering hill at the centre of the molecule's distorted parabolic potential. However, the nitrogen atom can quantum mechanically tunnel through the barrier, leading to two sets of energy levels, corresponding to oscillations on either one side of the hill or the other. This inversion is a vibrational transition, but the energy levels are so close together – due to the inversion being slowed down by the hindering potential, the nitrogen oscillates slowly from one side of the potential barrier to the other – that their frequencies lie in microwave region (Townes and Schawlow 1955).

nia it is possible to determine the corrections necessary to obtain true kinetic temperatures from observations. Explanations for rising rotational temperatures with increasing energy above the ground state are: the presence of kinetic temperature gradients, optically thick lines or subthermal excitation. Radiative transfer calculations (Walmley and Ungerechts 1983) predict that rotational temperatures approach the kinetic temperature with rising energy of metastable inversion doublets.

Observations of CO 1–0 and 2–1 transitions are also commonly used to determine molecular cloud temperatures. For this, the emitted intensity is assumed to equal the Planck intensity corresponding to the molecular cloud temperature. Put another way, the level populations of CO are thermalised and the optical depths of the rotational transitions are so large that essentially black body conditions prevail. However, the problem with this approach is the assumption that the cloud is extended relative to the beam of the observing telescope. Self-absorption effects can also influence the derived temperature. The ratio  $T_{\text{rot}}/T_{\text{kin}}$  is fairly insensitive to all astrophysical parameters, but observed values of  $T_{\text{rot}}$  need to be corrected for the depopulation effect, therefore, a constructive approach is to compare the temperatures derived for the same cloud using both  $\text{NH}_3$  and CO. For distant sources such as EC2 and EC1, beam dilution probably affects CO measurements, whereas the frequencies of  $\text{NH}_3$  metastable lines are close together, and should therefore yield a more reliable temperature.

Mauersberger et al. (1985) also state that the rotational temperature is generally less than the kinetic temperature, and that the relation between these quantities is weakly dependent on the density of molecular hydrogen. They confirm that CO data likely to be affected by self absorption, resulting in lower kinetic temperatures compared to  $\text{NH}_3$ , and go on to say that ammonia results, compared to other molecular studies, best reflect the gas kinetic temperatures in those denser parts of clouds where  $\text{NH}_3$  is present. As noted by many authors, the results for metastable emission of  $\text{NH}_3$  give support for a “clumpy-cloud” model if lines are thermalised, i.e.  $T_{\text{ex}} = T_{\text{kin}}$ .

### 9.3 Determination of temperature

From the above it is clear that the species most suited to a determination of kinetic temperature,  $T_{\text{kin}}$ , in EC2 is  $\text{NH}_3$ . Although CO must be thermalised, unknown beam filling factors for the optically thick 1–0 transition do not allow it to be used as a thermometer. Once having fixed  $T_{\text{kin}}$ , I will then use other tracers, those sensitive to both density and temperature, to determine the density of the gas.

At least four of the five groups of hyperfine components have been detected in the  $(J, K)=(1,1)$  line of  $\text{NH}_3$ , and the line intensity ratios are consistent with optically thin emission. Gaussian fits of the groups of hyperfine components are (with increasing velocity) 23.3, 17.2, 80.2, 5.7 and 11.1 mJy km s<sup>-1</sup> (see Fig. 8.6, the features being marked ‘HF’). For the (2,2) line I get  $38.0 \pm 8.0$  mJy km s<sup>-1</sup>. The (2,2)/(1,1) line intensity ratio is then  $0.28 \pm 0.07$ , with the error being dominated by the low signal-to-noise ratio of the (2,2) line. To derive total beam averaged column densities (cm<sup>-2</sup>) in an inversion doublet, I use

$$N(J, K) = 1.55 \times 10^{14} \frac{J(J+1)}{\nu K^2} \int T_{\text{mb}} dV \quad (9.10)$$

(equation 1 in Henkel et al. 2000) that is valid in the optically thin limit. For the inversion split of  $\text{NH}_3$  at 23.7 GHz,  $\Delta T$  is  $h\nu/k \sim 1.14$  K, which is significantly lower than expected excitation temperatures  $\gtrsim 10$  K, therefore the measured line intensities must be from inversion doublets. As the factor of  $7.77 \times 10^{13}$  in (Henkel et al. 2000) refers to the lower state only, it is therefore doubled in equation 9.10 above. The frequency  $\nu$ , and the integral are in units of GHz, and K km s<sup>-1</sup>, respectively. As already indicated in section 8.3, the conversion factor between the Jy and the  $T_{\text{mb}}$  scale is 1.4. Thus I obtain total beam averaged column densities of  $2.52 \times 10^{12}$  and  $5.21 \times 10^{11}$  cm<sup>-2</sup> in the (1,1) and (2,2) inversion doublets. The (2,2)/(1,1) column density ratio is then  $0.21 \pm 0.05$ .

Using equation 9.4 and assuming LTE, a Boltzmann distribution requires that the

ratio of column densities be

$$\frac{N_{(2,2)}}{N_{(1,1)}} = \frac{g_{op(2)}}{g_{op(1)}} \frac{g_2}{g_1} \exp(-\Delta E/kT), \quad (9.11)$$

where  $\Delta E$  is the energy difference between the (1,1) and (2,2) levels;  $g_{op(J)}$  is the statistical weight due to nuclear spin, being unity for para-ammonia ( $J, K$ ) = (1,1) and (2,2); and  $g_J = (2J + 1)$  is the statistical weight due to rotational degeneracy. Thus equation 9.11 becomes

$$\frac{N_{(2,2)}}{N_{(1,1)}} = (5/3) \exp(-\Delta E/kT), \quad (9.12)$$

and with  $\Delta E = 40.957k$  K (or  $28.465k$  cm<sup>-1</sup>,  $h\nu = 5.65 \times 10^{-15}$  erg,  $\nu \sim 853$  GHz) and a column density ratio of  $0.21 \pm 0.05$ , I derive a rotational temperature  $T_{rot} = 20 \pm 3$  K.

With a rotational temperature of 20 K the column density of the (0,0) level (single as it is not an inversion doublet), at 23.19 K below the (1,1) state, can be calculated by adapting equation 9.11 for the (1,1)/(0,0) column density ratio:

$$N_{(0,0)} = \frac{N_{(1,1)}}{3 \exp(-\Delta E/kT)}, \quad (9.13)$$

which yields a column density of  $2.73 \times 10^{12}$  cm<sup>-2</sup> for the (0,0) level. It should be noted that the (0,0) level is ortho-ammonia, which doubles its statistical weight ( $g_{op(0)} = 2$ ), but as there is only one state (i.e. no inversion doublet), this is then factored by 0.5. The total statistical weights ( $g_{op(J)}g_J$ ) are 1, 3 and 5 for the (0,0), (1,1) and (2,2) levels respectively. The total NH<sub>3</sub> column density, summed over the (0,0), (1,1) and (2,2) levels is  $N(\text{NH}_3) = 5.77 \times 10^{12}$  cm<sup>-2</sup>, with an uncertainty of  $\pm 15$  per cent, averaged over the 40'' beam.  $J > K$  levels require extremely high densities, (Mauersberger et al. 1985) and are therefore not relevant.

## 9.4 Determination of density

Using the rotational temperature derived in the previous section, which should be close to the kinetic temperature (Walmsley and Ungerechts 1983), the density of EC2 was estimated using Large Velocity Gradient (LVG) models for a number of molecular

species (Henkel 2006a), for a spherical cloud with constant density (see Henkel et al. 1980; Mauersberger et al. 1990, and references therein).

## H<sub>2</sub>CO

The EC2 H<sub>2</sub>CO data was reproduced using LVG models involving 40 ortho-H<sub>2</sub>CO states up to  $K_{a=3}$ , and the collision cross sections of Green (1991). Examining the CO maps for EC2 (section 8.6), I estimated a full width to half power source size,  $fwhp_s$ , of  $150 \times 40$  arcsec<sup>2</sup>. As discussed in section 9.1, applying this to the line intensities,  $T_R^*$ , gives correction factors,  $\eta_{bf}$ , and deconvolved line intensities,  $T_{mb}$ . A fit to the first two absorption lines,  $1_{10-1_{11}}$  (6cm) and  $2_{11-2_{12}}$  (2cm), gives a density of  $2.5 \times 10^4$  cm<sup>-3</sup>, but with the 2mm lines seen in emission coming out too strong (relative to the observations) by about 50 per cent.

However, the source size of  $150 \times 40$  arcsec<sup>2</sup> was based on the extent of the <sup>12</sup>CO 2–1 emission seen in the CO maps, but it appears more realistic to use the extent of the <sup>13</sup>CO emission, which lets us ‘see’ inside the cloud, as opposed to the <sup>12</sup>CO emission which is likely to be optically thick. Therefore, I estimate a source size of  $100 \times 30$  arcsec<sup>2</sup> based on the <sup>13</sup>CO 2–1 emission. Applying this to the  $1_{10-1_{11}}$ ,  $2_{11-2_{12}}$ ,  $2_{12-1_{11}}$  and  $2_{11-1_{10}}$  lines, the correction factors,  $\eta_{bf}$ , give line intensities,  $T_{mb}$ , for the 2cm and 2mm results that are then consistent with the LVG models, and hence the preferred solution, giving a density of  $n(\text{H}_2) = 1.2 \times 10^4$  cm<sup>-3</sup>.

## SO

Using the <sup>13</sup>CO 2–1 source size of  $100 \times 30$  arcsec<sup>2</sup> (successfully applied for H<sub>2</sub>CO above), gives deconvolved line intensities,  $T_{mb}$ , for the SO  $1_0-0_1$  and  $3_2-2_1$  lines that are consistent with model results that use the collisional rates of Green (1994) and  $n(\text{H}_2) = 1.4 \times 10^5$  cm<sup>-3</sup>. However, the resulting density is a full order of magnitude higher than for H<sub>2</sub>CO, leading to the conclusion that there must be a large amount of small scale clumping. An increase in  $T_{kin}$  – even to 500 K – is not sufficient to make

the SO  $3_2-2_1$  line stronger than the  $1_0-0_1$  line.

## CS

The CS  $2-1$  and  $3-2$  line temperatures,  $T_R^*$ , were deconvolved using the  $^{13}\text{CO}$   $2-1$  source size of  $100 \times 30$  arcsec<sup>2</sup>, resulting in values for  $T_{\text{mb}}$  that can be roughly fitted with the density of  $1.2 \times 10^4$  cm<sup>-3</sup> obtained for H<sub>2</sub>CO (using CS collisional rates from Turner et al. 1992). The resulting excitation is slightly below the measured one, but still well within the observational and deconvolution errors. Not unexpectedly (the  $2-1$  and  $3-2$  transitions are too close for a good excitation analysis), the line ratio is almost independent of density and temperature. To get very close to the calculated intensity ratio one has to diminish densities to almost  $10^3$  cm<sup>-3</sup> or the kinetic temperature to 11 K. Overall, the lines are excitationally too nearby to reveal decent constraints on density and kinetic temperature, but the density clearly matches the H<sub>2</sub>CO as opposed to the SO result.

## HCO<sup>+</sup>

Using collisional rates from Flower (1999), the model reproduces HCO<sup>+</sup>  $1-0$  deconvolved line temperatures (again with a cloud size of  $100 \times 30$  arcsec<sup>2</sup>) for both the H<sub>2</sub>CO and the SO densities. The  $J = 3-2$  line intensities appear to be consistent with the observed upper limit, at least in the case of the lower density.

## HCN

For the rotational HCN  $J = 1-0$  transition, the detected hyperfine structure is compatible with optically thin emission, and the fractional HCN abundance varies proportionally to the integrated line intensity, i.e. the sum of the three hyperfine components. Using collisional rates from Schöier et al. (2005), the  $1-0$  deconvolved line intensity was fitted first for the H<sub>2</sub>CO density of  $1.2 \times 10^4$  cm<sup>-3</sup>, and second for the SO density of  $1.4 \times 10^5$  cm<sup>-3</sup>. For HCN, the higher density is likely to be the correct one, as the high

dipole moment of HCN ( $\mu_D \sim 3$  Debye) requires higher densities for a balance between spontaneous emission and collisional excitation. With higher density, the HCN level populations cover a wider  $J$  range (and diminish populations in the  $J = 0$  and  $J = 1$  state). Thus one should expect, for the higher density solution to the observed HCN 1–0 line intensity, a higher overall HCN abundance. However, in the LVG model the opposite is true because at  $1.2 \times 10^4 \text{ cm}^{-3}$ , excitation is still near the 2.7 K background, while at  $1.4 \times 10^5 \text{ cm}^{-3}$ , excitation reaches a few degrees. Therefore, in the case of HCN, radio observations are mainly sensitive to high density gas.

## HNC

Using collisional rates from Schöier et al. (2005), the model reproduces HNC deconvolved line temperatures (for a cloud size of  $100 \times 30 \text{ arcsec}^2$ ) for both the  $\text{H}_2\text{CO}$  and the SO densities. HNC is a lot like HCN, but the chemistry suggests that the high density solution is preferable.

## $\text{N}_2\text{H}^+$

$\text{N}_2\text{H}^+$  was not detected, which is highly unusual and presumably a sign of N depletion. The  $3\sigma$  value is simulated using collision cross sections from Flower (1999), for both the high and the low density solutions. The  $3\sigma$  intensity limit was calculated using:

$$\Delta(\text{K}) = 3\sigma_{\text{mb}}(1 + \alpha)\sqrt{\Delta\nu/\Delta V}, \quad (9.14)$$

where  $\sigma_{\text{mb}}$  is the deconvolved intensity rms value for non-detections,  $\alpha$  is the calibration uncertainty taken to be 0.15,  $\Delta\nu$  and  $\Delta V$  are the spectral resolution and expected line-width ( $2 \text{ km s}^{-1}$  is assumed here), both measured in  $\text{km s}^{-1}$ .

## CO

Based on my CO maps (section 8.6), observed line intensities were deconvolved with a cloud of size of  $150 \times 40 \text{ arcsec}^2$  for  $^{12}\text{CO}$ , and  $100 \times 30 \text{ arcsec}^2$  for  $^{13}\text{CO}$  and

## 9: ANALYSIS OF EC2 OBSERVATIONS

$C^{18}O$ . As  $^{13}CO$  is assumed to be optically thin and was observed in three lines, the deconvolved  $^{13}CO$  intensities were fitted to an LVG model using collisional rates from Flower (2001) and an adopted ortho-para ratio of 3 for  $H_2$  (although the results are only weakly dependent on this), with a resulting density of  $n(H_2) = 3.2 \times 10^3 \text{ cm}^{-3}$ . With this density,  $C^{18}O$  (only two lines) and  $^{12}CO$  could then also be fitted. This gives abundance ratios of approximately 100:10:1 for  $^{12}CO:^{13}CO:C^{18}O$ . However, this can not reflect the actual abundance ratios, as the optically thin  $^{12}C/^{13}C$  ratio is  $\sim 89$  in the solar system, and 60 to 70 in diffuse clouds. The best fit also gives a fractional abundance with regard to  $H_2$  of  $\sim 10^{-7}$  for  $^{13}CO$ , well below the value of  $2 \times 10^{-6}$  typically found in local metal-rich molecular clouds. For the  $C^{18}O/H_2$  ratio the model gives  $\sim 10^{-8}$  compared to the local value of  $1.7 \times 10^{-7}$  with  $^{16}O/^{18}O = 500$  (Frerking et al. 1982).

There are several ways to explain these discrepancies: (i) optical thickness of  $^{12}CO$ ; (ii)  $^{13}CO$  enhancement by fractionation in cloud edges due to charge exchange reactions with  $C^+$  (e.g. Watson et al. 1976); (iii) small scale clumping, suggested by the  $H_2$  density derived from the SO line intensity ratio (discussed above), and in a similar situation for a different target, discussed extensively by Wang et al. (2004) in their section 4.1; or (iv) some combination of the above. The energy barrier for the fractionation reaction  $^{13}C^+ + ^{12}CO \longleftrightarrow ^{13}CO + ^{12}C^+$  is  $\sim 35 \text{ K}$ , which requires low temperatures, but low temperatures imply high  $A_V$  and hence little  $C^+$ . Also, for higher UV fields, where  $^{12}CO$  self-shields more effectively than  $^{13}CO$ , selective photodissociation destroys  $^{13}CO$  faster than  $^{12}CO$ . Column 13 in Table 9.4 lists optical depth values ( $\tau$ ) used in the LVG models, and it can be seen that the optical thickness of  $^{12}CO$  (and possibly  $^{13}CO$ ) has been taken into account when fitting observed intensities to the LVG model. Therefore I conclude fractionation to be unlikely, and that optical depth effects, enhanced by the clumpiness of EC2 (i.e. greater cloud surface area) to be the most likely explanation for the discrepancies.

## 9.5 Determination of molecular abundances

Table 9.3 lists column densities and abundances estimated with the methods described in this section, which presents an alternative approach to estimating molecular abundances to that of the LVG modelling described in the previous section. Table 9.4 shows good agreement between the two methods. In order to derive accurate molecular abundances one needs multiple transitions of a variety of isotopes to account for optical depth and excitation effects. Furthermore, the use of optically thin transitions of isotopes to derive accurate abundances of the main species is also fraught with difficulty since the underlying isotopic ratios may be different in this gas at the edge of the Galaxy than in the more local molecular clouds. To derive molecular abundances for species other than CO, H<sub>2</sub>CO and NH<sub>3</sub>, I have assumed LTE and an excitation temperature of 20 K. Most of the derived abundances are not very sensitive to temperature, typically varying by less than  $\pm 10$  per cent for  $T = 20 \pm 3$  K, except for detections of CO 3–2 ( $\pm 22\%$ ), C<sub>1</sub> ( $\pm 18\%$ ), SO ( $\pm 13\%$ ), H<sub>2</sub>CO ( $\pm 12\%$ ) and NH<sub>3</sub> ( $\pm 12\%$ ).<sup>2</sup>

For optically thin emission from linear molecules, I find that the total column density,  $N$ , of a molecule with normalised electric dipole moment  $\tilde{\mu}$  (in Debye) with an excitation temperature  $T_{\text{ex}}$  emitting at frequency  $\nu$  in a transition  $J \rightarrow J - 1$  can be written in the form:

$$N(\text{cm}^{-2}) = \frac{1.603 \times 10^{13} T_{\text{ex}}}{\tilde{\mu}^2 T_0^2} \exp[(J + 1)T_0/2T_{\text{ex}}] \int T_{\text{mb}} dV, \quad (9.15)$$

where  $T_0 = h\nu/k$  and the deconvolved integrated intensity for a Gaussian line profile is given by  $1.06 T_{\text{mb}} \Delta V$  in units of K km s<sup>-1</sup>. For non-detections I use the  $3\sigma$  upper limits for the integrated intensity:

$$\Delta(\text{K km s}^{-1}) = 3rm s_{\text{mb}}(1 + \alpha) \sqrt{\Delta\nu \Delta V}, \quad (9.16)$$

---

<sup>2</sup>For this reason I ignored the microwave background temperature,  $T_{\text{bg}}$ , and worked in the Rayleigh-Jeans approximation:  $J(T_{\text{ex}}) \rightarrow T_{\text{ex}}$  and  $Q(T_{\text{ex}}) \rightarrow T_{\text{ex}}/B$  (for a linear molecule) where  $B$  is the rotational constant in temperature units (equation 9.9). However,  $B$  is not needed explicitly since  $h\nu/k = 2BJ$  for a transition  $J \rightarrow J - 1$ .

where  $\alpha$  is the calibration uncertainty taken to be 0.15,  $\Delta\nu$  and  $\Delta V$  are the spectral resolution and expected line width (2 km s<sup>-1</sup> is adopted here), both measured in km s<sup>-1</sup>. Permanent electric dipole moments (where 1 Debye = 10<sup>-18</sup> esu) are listed in Appendix N. For CN I summed the intensities of the two observed hyperfine components and adopted a relative intensity of 0.456 to determine  $N(\text{CN})$ . For the rotational HCN 1–0 transition, the hyperfine structure is compatible with optically thin emission, so I summed the integrated intensities of the three hyperfine components, and then divided by the average of the line widths to get a peak intensity. For C<sub>2</sub>H, I used the strongest hyperfine component at 87.317 GHz and adopted a relative intensity of 0.4167 to determine the column density.

## SO

I take a slightly different approach for SO which has a <sup>3</sup>Σ ground state. I calculate  $N(\text{SO})$  directly using the formula given by Takano et al. (1995) with the partition function from the JPL Molecular Spectroscopy Catalogue (Pickett et al. 1998):

$$N(\text{SO}) = \left( \frac{3hQ}{8\pi^3\mu^2S} \right) \frac{1}{J(T_{\text{ex}}) - J(T_{\text{bg}})} \frac{1}{\exp(h\nu/kT_{\text{ex}}) - 1} \exp\left(\frac{E_u}{kT_{\text{ex}}}\right) \int T_{\text{mb}}dV, \quad (9.17)$$

where  $Q$  = partition function,  $\mu$  = dipole moment (in esu),  $S$  = line strength,  $E_u$  = energy of upper state, and  $J(T) = h\nu/k(e^{h\nu/kT} - 1)^{-1}$ . In the Rayleigh-Jeans limit ( $J(T) \rightarrow T$ ), this reduces to:

$$N(\text{SO}) = \left( \frac{3hQ}{8\pi^3\mu^2S} \right) \frac{1}{T_0} \exp\left(\frac{E_u}{kT_{\text{ex}}}\right) \int T_{\text{mb}}dV, \quad (9.18)$$

where  $T_0 = h\nu/k$ , and the partition function  $Q = 40$  at  $T_{\text{ex}} = 20$  K. Individual line parameters are: 1<sub>0</sub>–0<sub>1</sub>;  $E_u/k = 1.44$  K,  $S = 0.956$  and 3<sub>2</sub>–2<sub>1</sub>;  $E_u/k = 9.23$  K,  $S = 2.933$ . For linear molecules like SO,  $E_u/k = T_0(J + 1)/2$ . Note that in order to get a column density in units of cm<sup>-2</sup> the rhs of equation 9.18 must be multiplied by 10<sup>5</sup> to convert km s<sup>-1</sup> to cm s<sup>-1</sup>.

## C<sub>I</sub>

For C<sub>I</sub> I use a similar approach to that of Tauber et al. (1995):

$$N(\text{CI}) = \left( \frac{8k\pi\nu^2}{hc^3A_{10}} \right) \frac{Q(T_{\text{ex}})}{3} \exp\left(\frac{23.66}{T_{\text{ex}}}\right) \int T_{\text{mb}}dV, \quad (9.19)$$

where  $A_{10} = 7.9 \times 10^{-8} \text{ s}^{-1}$  (Einstein  $A$  coefficient for 492 GHz transition) and

$$Q(T_{\text{ex}}) = 1 + 3 \exp\left(\frac{-T_1}{T_{\text{ex}}}\right) + 5 \exp\left(\frac{-T_2}{T_{\text{ex}}}\right). \quad (9.20)$$

For  $T_{\text{ex}} = 20 \text{ K}$ ,  $Q = 2.139$ , where  $T_1 = 23.66 \text{ K}$  and  $T_2 = 62.5 \text{ K}$ . Tauber et al.'s formula incorporates this – so  $Q$  does not appear explicitly – and writes  $N(\text{CI})$  in a slightly different form (C<sub>I</sub> has a triplet ground state, so only has three energy levels).

## H<sub>2</sub>CO

To estimate  $N(\text{H}_2\text{CO})$  I use the LVG modelled density as follows:

$$N(\text{H}_2\text{CO}) = n(\text{H}_2\text{CO}) \times 1\text{pc} \times \Delta V, \quad (9.21)$$

where  $n(\text{H}_2\text{CO})$  is the best fit abundance to the LVG calculation ( $1.4 \times 10^{-6} \text{ cm}^{-3}$ ),  $1 \text{ pc} = 3.08 \times 10^{18} \text{ cm}$  and  $\Delta V = 1.3 \text{ km s}^{-1}$  (the  $1_{10} - 1_{11}$  line is widened by hyperfine structure). Note that as the LVG calculations are done in units of  $\text{km s}^{-1}$  it is not necessary to multiply by  $10^5$  to convert to  $\text{cm}^{-2}$ .

For the  $1_{1,0} - 1_{1,1}$  transition at 4.83 GHz, an alternative approach is provided by Henkel (2006b):

$$N_{1_{1,1}} = 1.61 \times 10^{12} \frac{1}{J(T_{\text{ex}}) - J(T_{\text{bg}})} \frac{1}{1 - \exp(-h\nu/kT_{\text{ex}})} \int T_{\text{mb}}dV, \quad (9.22)$$

where  $J(T) \rightarrow T$  in the Rayleigh-Jeans limit. The total column density,  $N$ , is then calculated using equation 9.8, with

$$Q_{\text{rot}} = \frac{1}{2} \left[ \frac{\pi(kT)^3}{h^3ABC} \right]^{1/2} \quad (9.23)$$

and an additional reduced nuclear spin degeneracy factor,  $g_I = 3/4$  (ortho), from Turner (1991), and values for the rotation constants  $A$ ,  $B$  and  $C$  from Townes and Schawlow (1955). This latter approach gives a value of  $3.85 \times 10^{13} \text{ cm}^{-2}$ , which is  $\sim 7$  times more than the value of  $5.61 \pm 1.2 \times 10^{12} \text{ cm}^{-2}$  derived from the LVG model.

### Column density errors

For detected lines, I calculated the error on the column density by noting that the value of  $N$  is proportional to  $T_{\text{mb}}\Delta V$ , thus the error on  $N$  is the addition in quadrature of the errors in  $T_{\text{mb}}$  and  $\Delta V$ , i.e.

$$(\sigma_N/N)^2 = (\sigma_{T_{\text{mb}}}/T_{\text{mb}})^2 + (\sigma_{\Delta V}/\Delta V)^2, \quad (9.24)$$

which gives

$$\sigma_N = N \sqrt{(\sigma_{T_{\text{mb}}}/T_{\text{mb}})^2 + (\sigma_{\Delta V}/\Delta V)^2}, \quad (9.25)$$

where  $T_{\text{mb}}$  is the deconvolved peak intensity,  $\sigma_{T_{\text{mb}}}$  is the baseline rms value  $rms_{\text{mb}}$ ,  $\Delta V$  is the Gaussian *fwhp* line width and  $\sigma_{\Delta V}$  is the error on the line width.

### Comparison of derived column densities

Table 9.4 compares line temperatures and column densities for EC2 derived from observed deconvolved integrated intensities and the LVG models, and it can be seen that in most cases there is good agreement between  $N_{\text{mb}}(\text{X})$  and  $N_{\text{lvG}}(\text{X})$ . The LVG column densities were calculated from the best fit model densities with  $N_{\text{lvG}}(\text{X}) = n_{\text{lvG}}(\text{X}) \times 1 \text{ pc} \times \Delta V$ .

## 9.6 Determination of dust to gas ratio and mass

Dust emission can be used to estimate the mass of cold molecular clouds, and I now use my detected peak continuum emission at 1.2 mm (section 8.7) to calculate the opacity and dust to gas ratio in EC2. First, I estimate  $\tau_\nu$ , the dust opacity at frequency  $\nu$ , using

$$\tau_\nu = B(\nu)/\pi(\theta_b/2)^2 B_\nu(T_{\text{dust}}), \quad (\tau \ll 1) \quad (9.26)$$

from Hildebrand (1983), where  $B_\nu(T_{\text{dust}})$  is the Planck function:

$$B_\nu(T_{\text{dust}}) = \frac{2h}{c^2} \frac{\nu^3}{\exp(h\nu/kT_{\text{dust}}) - 1} \text{ Jy sr}^{-1}, \quad (9.27)$$

where  $T_{\text{dust}} = 20 \text{ K}$ , the observed dust emission  $B(\nu) = 20.3 \times 10^{-3} \text{ Jy}$ , and the beam size  $\theta_b = 11'' = 5.333 \times 10^{-5} \text{ rad}$ , which gives a value of  $\tau_\nu = 3.25 \times 10^{-4}$ . Next, I calculate  $\kappa_\nu$ , the dust opacity per unit mass column density at frequency  $\nu$ :

$$\kappa_\nu = \frac{3}{4} \frac{Q_\nu}{a\rho}, \quad (9.28)$$

where  $Q_\nu$  is the dust emissivity which varies as  $\nu^\beta$  [ $B(\nu) \propto \nu^\beta B_\nu(T_{\text{dust}})$ ], the average dust grain radius  $a = 0.1 \mu\text{m}$ , and the density of the dust  $\rho = 3 \text{ g cm}^{-3}$ . Values for  $Q_\nu$ ,  $a$  and  $\rho$  are taken from the *1983 Chicago Assumptions* of Hildebrand (1983). From Whittet (1992, p150) I note that the average density of dust in a column of length  $L$  can be estimated from the relation:

$$\rho_{\text{dust}} = \tau_\nu / \kappa_\nu L, \quad (9.29)$$

where  $L = D \tan \theta_b$ , and  $D$  is the distance of EC2 (14–20 kpc). It follows that the dust mass,  $M_{\text{dust}} = \rho_{\text{dust}} V$ , where  $V = (4/3)\pi(L/2)^3$ . For the same beam size,  $\theta_b$ , the gas mass,  $M_{\text{gas}} = Vn(\text{H}_2)\mu m_{\text{H}}$ , where  $n(\text{H}_2) = 1.2 \times 10^4 \text{ cm}^{-3}$  is my derived density, with a mean molecular weight  $\mu = 2.33$ , and an atomic hydrogen mass  $m_{\text{H}} = 1.67 \times 10^{-24} \text{ g}$ . Combining the above, the dust to gas ratio is therefore:

$$\frac{M_{\text{dust}}}{M_{\text{gas}}} = \frac{\tau_\nu}{\kappa_\nu L n(\text{H}_2)\mu m_{\text{H}}}, \quad (9.30)$$

## 9: ANALYSIS OF EC2 OBSERVATIONS

and Table 9.1 lists derived dust to gas ratios for  $D = 14$  and  $20$  kpc, and a range of values for  $\beta$  from 1 to 2, as well as appropriate values for  $Q_{1200}$  and  $\kappa_v$ . (Alternative methods of estimating dust mass can be found in Pagani et al. (2004) and Mookerjee et al. (2004), although I note that they assume the standard dust to gas ratio of 0.01.)

It now remains to relate the dust to gas ratio to possible values of extinction in EC2. For the standard dust to gas ratio of 1 per cent in the local ISM, it is found that  $N(\text{H})/E(B - V) = 5.8 \times 10^{21}$  atoms  $\text{cm}^{-2}$  mag $^{-1}$  (Bohlin et al. 1978). Assuming the standard interstellar value for the ratio of visual extinction to colour excess,  $R_V = A_V/E(B - V) = 3.1$ ,  $N(\text{H})/A_V = 1.9 \times 10^{21}$  atoms  $\text{cm}^{-2}$  mag $^{-1}$ . For different values of the dust to gas ratio, the visual extinction,  $A_V$ , scales linearly and can therefore be estimated using:

$$A_V = \frac{2n(\text{H}_2)L}{N(\text{H})/A_V} \frac{M_{\text{dust}}/M_{\text{gas}}}{0.01}, \quad (9.31)$$

and appropriate values from above. However, as discussed in chapter 6 (see also Ruffle et al. 2004), the value of  $R_V$  may be lower in certain regions of the ISM, so I calculate values of  $A_V$  for  $R_V = 3.1$  and  $R_V = 2.0$ , and the results are included in Table 9.1. It should be noted that values for  $A_V$  are insensitive to the distance of EC2 or the adopted density, as the extinction is determined solely by the amount of dust in the beam. As my CO maps show, EC2 is clumpy in structure and the peak dust detection of 20.3 mJy/beam(11'') traces the peak CO emission of one such clump. However, the rms

Table 9.1: Range of dust to gas ratios and extinction for EC2 based on  $D$  and  $\beta$ .

$\beta$	1	1.25	1.5	1.75	2
$Q_{1200}$	7.81e-5	4.44e-5	2.52e-5	1.43e-5	8.14e-6
$\kappa_v$ ( $\text{cm}^2 \text{g}^{-1}$ )	1.953	1.110	0.630	0.358	0.203
$M_{\text{dust}}/M_{\text{gas}}$ ( $D = 14$ kpc)	0.0015	0.0027	0.0048	0.0084	0.0148
$M_{\text{dust}}/M_{\text{gas}}$ ( $D = 20$ kpc)	0.0011	0.0019	0.0033	0.0059	0.0104
$A_V$ (mag) ( $R_V = 3.1$ )	4.6	8.0	14.1	24.9	43.8
$A_V$ (mag) ( $R_V = 2.0$ )	2.9	5.2	9.1	16.1	28.3

$Q_v$  and  $\kappa_v$  calculated from the *1983 Chicago Assumptions* of Hildebrand (1983).

## 9.6: DETERMINATION OF DUST TO GAS RATIO AND MASS

value of 6.35 mJy/beam(11'') is  $\sim 3$  times less than the peak, so extinction in EC2 as a whole is likely to be correspondingly lower.

Finally, I estimate upper and lower limits for the mass of EC2 based on a density of  $n(\text{H}_2) = 1.2 \times 10^4 \text{ cm}^{-3}$ . From Fig. 8.14, I estimate a cloud size of around  $600'' \times 300''$ , which equates to a notional cloud diameter of  $424''$ , which yields a mass range of  $8.4 \times 10^6 M_\odot$  to  $2.4 \times 10^7 M_\odot$  for the distance range 14–20 kpc. Taking the clumpy structure of EC2 into account, the average density may be of the order  $n(\text{H}_2) = 10^3 \text{ cm}^{-3}$ , so my initial mass estimate is  $M_{\text{EC2}} \sim 10^6 M_\odot$ . This value can be compared with a virial mass estimate using the method of MacLaren et al. (1988, equation 3):

$$M_{\text{vir}}/M_\odot = k_2 r \Delta V^2, \quad (9.32)$$

where  $k_2 = 190$  (for  $\rho \propto 1/r$ ),  $r$  is the radius of the cloud in pc, and  $\Delta V$  is the  $^{13}\text{CO}$  line width (FWHM) in  $\text{km s}^{-1}$  (as the optically thin  $^{13}\text{CO}$  line samples velocities throughout the cloud). For the distance range 14–20 kpc, the cloud radius,  $r$  is 14–21 pc and the line width for the strongest  $^{13}\text{CO}$  2–1 transition is  $1.87 \text{ km s}^{-1}$ , which yields a virial mass  $M_{\text{vir}} \sim 10^4 M_\odot$ , similar to the estimate of  $2.1 \times 10^4 M_\odot$  by Digel et al. (1994), but two orders of magnitude less than my direct estimate above (based on their CO detections Digel et al. estimated  $M_{\text{EC2}} = 3.7 \times 10^4 M_\odot$ ).

However, a more conservative interpretation of my CO 2–1 maps of EC2 (Fig. 8.14) would be that the cloud consists of two dense clumps  $\sim 75''$  in diameter, which for  $n(\text{H}_2) = 10^3 \text{ cm}^{-3}$  yields a gas mass of  $\sim 10^4 M_\odot$ , and a virial mass of  $\sim 10^3 M_\odot$ , thereby reducing the mass discrepancy to around one order of magnitude (as  $M_{\text{gas}} \propto r^3$  and  $M_{\text{vir}} \propto r$ , any overestimate of  $r$  is going to lead to a greater discrepancy between the two values). Taking the clumpy structure of EC2 into account, I would therefore suggest a mass estimate of  $M_{\text{EC2}} \approx 10^4 M_\odot$  as more realistic. The lower virial mass suggests that the cloud is gravitationally unstable and a likely site of star formation as suggested by the observations of Kobayashi and Tokunaga (2000).

9: ANALYSIS OF EC2 OBSERVATIONS

Table 9.2: Summary of observations and detections toward EC2 position A, with  $T_R^*$  beam deconvolved to yield  $T_{mb}$  intensities (see sections 8.3 and 9.1).

Molecule	Transition	Freq. (GHz)	Telescope	$T_R^*$	$rms_R^*$ (K)	$T_{mb}$	$rms_{mb}$ (K)
CO <sup>b</sup>	1-0	115.271	ARO 12m	5.257	0.101	7.863	0.151
<sup>13</sup> CO	1-0	110.201	ARO 12m	0.719	0.063	1.499	0.131
C <sup>18</sup> O	1-0	109.782	ARO 12m	0.057	0.013	0.119	0.027
C <sup>17</sup> O	1-0	112.359	ARO 12m	—	0.006	—	0.012
CO	2-1	230.538	JCMT 15m	5.827	0.024	6.289	0.026
<sup>13</sup> CO	2-1	220.399	JCMT 15m	1.616	0.062	1.897	0.073
C <sup>18</sup> O	2-1	219.560	JCMT 15m	0.142	0.031	0.167	0.036
CO	3-2	345.796	JCMT 15m	3.588	0.019	3.715	0.020
<sup>13</sup> CO	3-2	330.588	JCMT 15m	0.665	0.025	0.716	0.027
C <sup>18</sup> O	3-2	329.330	JCMT 15m	—	0.020	—	0.022
C <sub>I</sub>	<sup>3</sup> P <sub>1</sub> - <sup>3</sup> P <sub>0</sub>	492.161	JCMT 15m	2.275	0.398	2.354	0.412
CS	2-1	97.981	ARO 12m	0.124	0.013	0.294	0.031
CS	3-2	146.969	ARO 12m	0.044	0.008	0.071	0.013
C <sup>34</sup> S	3-2	144.617	ARO 12m	—	0.009	—	0.015
CN	1, $\frac{3}{2}, \frac{3}{2}-0, \frac{1}{2}, \frac{1}{2}$	113.488	ARO 12m	0.016	0.004	0.032	0.008
CN	1, $\frac{3}{2}, \frac{5}{2}-0, \frac{1}{2}, \frac{3}{2}$	113.491	ARO 12m	0.021	0.004	0.042	0.008
SO	1 <sub>0</sub> -0 <sub>1</sub>	30.002	MPIfR 100m	0.074	0.014	0.095	0.018
SO	3 <sub>2</sub> -2 <sub>1</sub>	99.300	ARO 12m	0.057	0.007	0.133	0.016
DCO <sup>+</sup>	1-0	72.039	ARO 12m	—	0.005	—	0.018
H <sup>13</sup> CO <sup>+</sup> <sup>a</sup>	1-0	86.754	ARO 12m	—	0.007	—	0.019
HCO <sup>+</sup>	1-0	89.189	ARO 12m	0.132	0.013	0.351	0.035
HCO <sup>+</sup>	3-2	267.558	JCMT 15m	—	0.012	—	0.013
DCN <sup>a</sup>	1-0	72.415	ARO 12m	—	0.042	—	0.148
H <sup>13</sup> CN	1-0	86.340	ARO 12m	—	0.005	—	0.014
HCN	1-0	88.634	ARO 12m	0.102	0.012	0.274	0.032
HNC	1-0	90.664	ARO 12m	0.032	0.007	0.083	0.018
C <sub>2</sub> D <sup>a</sup>	1-0	72.108	ARO 12m	—	0.006	—	0.021
C <sub>2</sub> H	1-0	87.317	ARO 12m	0.073	0.007	0.199	0.019
C <sub>2</sub> H	1-0	87.329	ARO 12m	0.031	0.007	0.085	0.019
N <sub>2</sub> H <sup>+</sup>	1-0	93.174	ARO 12m	—	0.008	—	0.020
H <sub>2</sub> CO	1 <sub>1,0</sub> -1 <sub>1,1</sub>	4.830	MPIfR 100m	-0.028	0.006	-0.256	0.055
H <sub>2</sub> CO	2 <sub>1,1</sub> -2 <sub>1,2</sub>	14.488	MPIfR 100m	-0.011	0.006	-0.021	0.011
H <sub>2</sub> CO	2 <sub>1,2</sub> -1 <sub>1,1</sub>	140.840	ARO 12m	0.051	0.013	0.085	0.022
H <sub>2</sub> CO	2 <sub>1,1</sub> -1 <sub>1,0</sub>	150.498	ARO 12m	0.034	0.005	0.054	0.008
HDCO <sup>a</sup>	2 <sub>1,1</sub> -1 <sub>1,0</sub>	134.285	ARO 12m	—	0.007	—	0.012
NH <sub>3</sub>	1-1	23.694	MPIfR 100m			0.040	0.006
NH <sub>3</sub>	2-2	23.723	MPIfR 100m			0.015	0.005
HC <sub>3</sub> N	9-8	81.881	ARO 12m	—	0.007	—	0.021
C <sub>3</sub> H <sub>2</sub>	2 <sub>1,2</sub> -1 <sub>0,1</sub>	85.338	ARO 12m	0.035	0.014	0.098	0.039
CH <sub>3</sub> OH	2 <sub>-1</sub> -1 <sub>-1</sub> E	96.739	ARO 12m	0.025	0.005	0.060	0.012
CH <sub>3</sub> OH	2 <sub>0</sub> -1 <sub>0</sub> A <sup>+</sup>	96.741	ARO 12m	0.018	0.005	0.043	0.012

<sup>a</sup> Feb 2005, <sup>b</sup> Jan 2006. All other ARO 12m detections June 2002.

9.6: DETERMINATION OF DUST TO GAS RATIO AND MASS

Table 9.3: Summary of column densities and abundances toward EC2 position A, estimated for an excitation temperature of 20 K (see section 9.5).

Molecule	Transition	$\Delta V$ (km s <sup>-1</sup> )	$\Delta \nu$ (km s <sup>-1</sup> )	$N$ (cm <sup>-2</sup> )	X/HCO <sup>+</sup>	X/H <sub>2</sub>
CO <sup>b</sup>	1-0	2.70 ± 0.04	0.650	2.48 ± 0.06 × 10 <sup>16</sup>	17078	3.3 × 10 <sup>-7</sup>
<sup>13</sup> CO	1-0	2.24 ± 0.13	0.272	4.24 ± 0.45 × 10 <sup>15</sup>	2919	5.7 × 10 <sup>-8</sup>
C <sup>18</sup> O	1-0	2.05 ± 0.41	0.683	3.11 ± 0.94 × 10 <sup>14</sup>	214	4.2 × 10 <sup>-9</sup>
C <sup>17</sup> O	1-0	—	0.667	<5.62 × 10 <sup>13</sup>	<38.8	<7.6 × 10 <sup>-10</sup>
CO	2-1	2.76 ± 0.01	0.406	8.81 ± 0.05 × 10 <sup>15</sup>	6070	1.2 × 10 <sup>-7</sup>
<sup>13</sup> CO	2-1	1.87 ± 0.06	0.425	1.90 ± 0.09 × 10 <sup>15</sup>	1308	2.6 × 10 <sup>-8</sup>
C <sup>18</sup> O	2-1	1.48 ± 0.32	0.427	1.33 ± 0.41 × 10 <sup>14</sup>	92	1.8 × 10 <sup>-9</sup>
CO	3-2	2.56 ± 0.01	0.542	4.92 ± 0.03 × 10 <sup>15</sup>	3389	6.6 × 10 <sup>-8</sup>
<sup>13</sup> CO	3-2	1.69 ± 0.06	0.567	6.37 ± 0.33 × 10 <sup>14</sup>	439	8.6 × 10 <sup>-9</sup>
C <sup>18</sup> O	3-2	—	0.569	<3.94 × 10 <sup>13</sup>	<27.2	<5.3 × 10 <sup>-10</sup>
Cl	<sup>3</sup> P <sub>1</sub> - <sup>3</sup> P <sub>0</sub>	2.23 ± 0.16	0.190	7.69 ± 1.45 × 10 <sup>16</sup>	53020	1.0 × 10 <sup>-6</sup>
CS	2-1	2.02 ± 0.17	0.306	3.38 ± 0.45 × 10 <sup>12</sup>	2.33	4.6 × 10 <sup>-11</sup>
CS	3-2	1.47 ± 0.22	0.510	3.75 ± 0.88 × 10 <sup>11</sup>	0.26	5.1 × 10 <sup>-12</sup>
C <sup>34</sup> S	3-2	—	0.207	<1.13 × 10 <sup>11</sup>	<0.08	<1.5 × 10 <sup>-12</sup>
CN	1, $\frac{3}{2}, \frac{3}{2}-0, \frac{1}{2}, \frac{1}{2}$	1.64 ± 0.40	0.660	2.29 ± 0.80 × 10 <sup>12</sup>	1.58	3.1 × 10 <sup>-11</sup>
CN	1, $\frac{3}{2}, \frac{5}{2}-0, \frac{1}{2}, \frac{3}{2}$	2.18 ± 0.38	0.660			
SO	1 <sub>0</sub> -0 <sub>1</sub>	1.80 ± 0.27	0.390	1.88 ± 0.45 × 10 <sup>13</sup>	13.0	2.5 × 10 <sup>-10</sup>
SO	3 <sub>2</sub> -2 <sub>1</sub>	1.95 ± 0.17	0.302	4.17 ± 0.63 × 10 <sup>12</sup>	2.87	5.6 × 10 <sup>-11</sup>
DCO <sup>+</sup>	1-0	—	0.416	<1.17 × 10 <sup>11</sup>	<0.08	<1.6 × 10 <sup>-12</sup>
H <sup>13</sup> CO <sup>+</sup> <sup>a</sup>	1-0	—	0.346	<8.27 × 10 <sup>10</sup>	<0.06	<1.1 × 10 <sup>-12</sup>
HCO <sup>+</sup>	1-0	2.74 ± 0.27	0.840	1.45 ± 0.20 × 10 <sup>12</sup>	1.00	2.0 × 10 <sup>-11</sup>
HCO <sup>+</sup>	3-2	—	0.350	<1.79 × 10 <sup>10</sup>	<0.01	<2.4 × 10 <sup>-13</sup>
DCN <sup>a</sup>	1-0	—	0.414	<1.65 × 10 <sup>12</sup>	<1.13	<2.2 × 10 <sup>-11</sup>
H <sup>13</sup> CN	1-0	—	0.347	<1.03 × 10 <sup>11</sup>	<0.07	<1.4 × 10 <sup>-12</sup>
HCN	1-0	1.54 ± 0.37	0.338	1.10 ± 0.30 × 10 <sup>12</sup>	0.76	1.5 × 10 <sup>-11</sup>
HNC	1-0	1.74 ± 0.42	0.331	3.48 ± 1.13 × 10 <sup>11</sup>	0.24	4.7 × 10 <sup>-12</sup>
C <sub>2</sub> D <sup>a</sup>	1-0	—	0.416	<3.32 × 10 <sup>12</sup>	<2.29	<4.5 × 10 <sup>-11</sup>
C <sub>2</sub> H	1-0	2.89 ± 0.23	0.858	5.15 ± 0.64 × 10 <sup>13</sup>	35.5	7.0 × 10 <sup>-10</sup>
C <sub>2</sub> H	1-0	1.86 ± 0.35	0.858			
N <sub>2</sub> H <sup>+</sup>	1-0	—	0.322	<9.67 × 10 <sup>10</sup>	<0.07	<1.3 × 10 <sup>-12</sup>
H <sub>2</sub> CO	1 <sub>1,0</sub> -1 <sub>1,1</sub>	3.20	0.303	5.61 ± 1.20 × 10 <sup>12</sup>	3.87	7.6 × 10 <sup>-11</sup>
H <sub>2</sub> CO	2 <sub>1,1</sub> -2 <sub>1,2</sub>	1.30	1.515			
H <sub>2</sub> CO	2 <sub>1,2</sub> -1 <sub>1,1</sub>	2.48 ± 0.47	0.532			
H <sub>2</sub> CO	2 <sub>1,1</sub> -1 <sub>1,0</sub>	1.83 ± 0.24	0.498			
HDCO <sup>a</sup>	2 <sub>1,1</sub> -1 <sub>1,0</sub>	—	0.223	<6.44 × 10 <sup>10</sup>	<0.04	<8.7 × 10 <sup>-13</sup>
NH <sub>3</sub>	1-1	2.00	0.500	5.77 ± 0.87 × 10 <sup>12</sup>	4.0	7.8 × 10 <sup>-11</sup>
NH <sub>3</sub>	2-2	2.60	0.500			
HC <sub>3</sub> N	9-8	—	0.366	<2.62 × 10 <sup>11</sup>	<0.18	<3.5 × 10 <sup>-12</sup>
C <sub>3</sub> H <sub>2</sub>	2 <sub>1,2</sub> -1 <sub>0,1</sub>	1.92 ± 0.47	0.351			
CH <sub>3</sub> OH	2 <sub>-1</sub> -1 <sub>-1</sub> E	0.93 ± 0.15	0.310			
CH <sub>3</sub> OH	2 <sub>0</sub> -1 <sub>0</sub> A <sup>+</sup>	1.49 ± 0.22	0.310			

<sup>a</sup> Feb 2005, <sup>b</sup> Jan 2006. All other ARO 12m detections June 2002.

Table 9.4: Comparison of line temperatures and column densities for EC2 derived from observed deconvolved integrated intensities and Large Velocity Gradient (LVG) models, as described in sections 9.4 and 9.5.

Molecule and Transition	Freq. (GHz)	$rm_{\text{mb}}$ (K)	$T_{\text{mb}}$ (K)	$T_{\text{lv}}$ (K)	$N_{\text{mb}}(X)$	$N_{\text{lv}}/N_{\text{mb}}$	$N_{\text{lv}}(X)$	$n_{\text{lv}}(X)$	$n(\text{H}_2)$	$n(X)/n(\text{H}_2)$	$\tau$	$T_{\text{ex}}$ (K)
CO 1-0	115.271	0.151	7.863	7.850	$2.48 \times 10^{16}$	1.0	$2.50 \times 10^{16}$	$3.00 \times 10^{-3}$	$3.20 \times 10^3$	$9.38 \times 10^{-7}$	0.622	20.40
$^{13}\text{CO}$ 1-0	110.201	0.131	1.499	1.500	$4.24 \times 10^{15}$	0.7	$2.76 \times 10^{15}$	$4.00 \times 10^{-4}$	$3.20 \times 10^3$	$1.25 \times 10^{-7}$	0.056	30.90
$\text{C}^{18}\text{O}$ 1-0	109.782	0.027	0.119	0.124	$3.11 \times 10^{14}$	0.6	$1.96 \times 10^{14}$	$3.10 \times 10^{-5}$	$3.20 \times 10^3$	$9.69 \times 10^{-9}$	0.004	37.50
CO 2-1	230.538	0.026	6.289	7.720	$8.81 \times 10^{15}$	2.9	$2.55 \times 10^{16}$	$3.00 \times 10^{-3}$	$3.20 \times 10^3$	$9.38 \times 10^{-7}$	2.220	13.60
$^{13}\text{CO}$ 2-1	220.399	0.073	1.897	1.810	$1.90 \times 10^{15}$	1.2	$2.31 \times 10^{15}$	$4.00 \times 10^{-4}$	$3.20 \times 10^3$	$1.25 \times 10^{-7}$	0.388	10.20
$\text{C}^{18}\text{O}$ 2-1	219.560	0.036	0.167	0.157	$1.33 \times 10^{14}$	1.1	$1.42 \times 10^{14}$	$3.10 \times 10^{-5}$	$3.20 \times 10^3$	$9.69 \times 10^{-9}$	0.033	9.42
CO 3-2	345.796	0.020	3.715	3.760	$4.92 \times 10^{15}$	4.8	$2.37 \times 10^{16}$	$3.00 \times 10^{-3}$	$3.20 \times 10^3$	$9.38 \times 10^{-7}$	2.120	10.50
$^{13}\text{CO}$ 3-2	330.588	0.027	0.716	0.699	$6.37 \times 10^{14}$	3.3	$2.09 \times 10^{15}$	$4.00 \times 10^{-4}$	$3.20 \times 10^3$	$1.25 \times 10^{-7}$	0.271	8.62
$\text{C}^{18}\text{O}$ 3-2	329.330	0.022	—	0.056	$3.94 \times 10^{13}$	4.9	$1.91 \times 10^{14}$	$3.10 \times 10^{-5}$	$3.20 \times 10^3$	$9.69 \times 10^{-9}$	0.020	8.44
CS 2-1	97.981	0.031	0.294	0.297	$3.38 \times 10^{12}$	6.8	$2.31 \times 10^{13}$	$3.70 \times 10^{-6}$	$1.20 \times 10^4$	$3.08 \times 10^{-10}$	1.370	3.22
CS 3-2	146.969	0.013	0.071	0.071	$3.75 \times 10^{11}$	45	$1.68 \times 10^{13}$	$3.70 \times 10^{-6}$	$1.20 \times 10^4$	$3.08 \times 10^{-10}$	5.620	3.00
SO $1_0-0_1$	30.002	0.018	0.095	0.096	$1.88 \times 10^{13}$	0.2	$3.11 \times 10^{12}$	$5.60 \times 10^{-7}$	$1.40 \times 10^5$	$4.00 \times 10^{-12}$	-0.017	-2.83
SO $3_2-2_1$	99.300	0.016	0.133	0.129	$4.17 \times 10^{12}$	0.8	$3.37 \times 10^{12}$	$5.60 \times 10^{-7}$	$1.40 \times 10^5$	$4.00 \times 10^{-12}$	0.045	6.62
$\text{HCO}^+$ 1-0	89.189	0.035	0.351	0.346	$1.45 \times 10^{12}$	1.9	$2.70 \times 10^{12}$	$3.20 \times 10^{-7}$	$1.20 \times 10^4$	$2.67 \times 10^{-11}$	0.659	3.57
HCN 1-0	88.634	0.032	0.274	0.274	$1.10 \times 10^{12}$	0.9	$9.50 \times 10^{11}$	$2.00 \times 10^{-7}$	$1.40 \times 10^5$	$1.43 \times 10^{-12}$	0.079	4.50
HNC 1-0	90.664	0.018	0.083	0.080	$3.48 \times 10^{11}$	7.7	$2.68 \times 10^{12}$	$5.00 \times 10^{-7}$	$1.20 \times 10^4$	$4.17 \times 10^{-11}$	0.656	2.93
$\text{N}_2\text{H}^+$ 1-0	93.174	0.020	—	0.028	$9.67 \times 10^{10}$	1.8	$1.70 \times 10^{11}$	$2.75 \times 10^{-8}$	$1.20 \times 10^4$	$2.29 \times 10^{-12}$	0.142	3.51
$\text{H}_2\text{CO}$ $1_{1,0}-1_{1,1}$	4.830	0.055	-0.256	-0.250	$5.61 \times 10^{12}$	2.5	$1.38 \times 10^{13}$	$1.40 \times 10^{-6}$	$1.20 \times 10^4$	$1.17 \times 10^{-10}$	0.152	0.95
$\text{H}_2\text{CO}$ $2_{1,1}-2_{1,2}$	14.488	0.011	-0.021	-0.021	—	1.0	$5.61 \times 10^{12}$	$1.40 \times 10^{-6}$	$1.20 \times 10^4$	$1.17 \times 10^{-10}$	0.016	1.43
$\text{H}_2\text{CO}$ $2_{1,2}-1_{1,1}$	140.840	0.022	0.085	0.096	—	1.9	$1.07 \times 10^{13}$	$1.40 \times 10^{-6}$	$1.20 \times 10^4$	$1.17 \times 10^{-10}$	0.623	3.05
$\text{H}_2\text{CO}$ $2_{1,1}-1_{1,0}$	150.498	0.008	0.054	0.049	—	1.4	$7.90 \times 10^{12}$	$1.40 \times 10^{-6}$	$1.20 \times 10^4$	$1.17 \times 10^{-10}$	0.501	2.94

Note: LVG column densities calculated with  $N_{\text{lv}}(X) = n_{\text{lv}}(X) \times 1 \text{ pc} \times \Delta V$ .